Available online at www.sciencedirect.com
SCIENCE DIRECT®
Polymer 45 (2004) 3555–3564
polymer
www.elsevier.com/locate/polymer

Effect of absorbed water on oxygen transport in EVOH matrices. A molecular dynamics study

Esra Kucukpinar, Pemra Doruker*

Department of Chemical Engineering and Polymer Research Center, Bogazici University, Bebek, Istanbul 34342, Turkey

Received 15 January 2004; received in revised form 5 March 2004; accepted 7 March 2004

Abstract

We performed molecular dynamics simulations on oxygen transport in dry and hydrated (with 3 and 13 wt% water content) amorphous ethylene-vinyl alcohol (EVOH) copolymers. As the water content increases, the intermolecular hydrogen bonding in the matrix decreases and the cavity sizes increase, which result in increased diffusion coefficients. The local chain mobility increases significantly only at 13% water content. The predicted glass transition temperatures fall into reported experimental ranges. The solubility coefficients of oxygen slightly decrease with increasing water content, which indicates that the excessive increase in permeability mainly results from increased diffusion rates.

Keywords: Gas diffusion; Glass transition; Local mobility

1. Introduction

Ethylene-vinyl alcohol (EVOH) copolymers are a family of resins with excellent barrier properties. They are used in the food packaging industry as gas-barrier materials for foods that are sensitive to certain levels of oxygen or carbon dioxide. The permeability of semi-crystalline EVOH depends on the copolymerization ratio of ethylene and vinyl alcohol. As the ethylene content increases, the permeability of EVOH increases. On the other hand, if the ethylene content is decreased to a value of 20 mol%, EVOH loses its process ability for practical applications. EVOH polymers with 25–45 mol% ethylene are considered to have the superior gas barrier properties compared to most of the polymeric materials [1].

One very big disadvantage of the EVOH copolymers is that they are very sensitive to moisture and they lose much of their barrier properties at high values of relative humidity [1]. Besides the increase in the permeability values of EVOH due to water absorption at high relative humidity conditions, their thermal and mechanical properties are also affected. The effect of water absorption both on the glass transition temperature (T_g) and on the oxygen and water vapor permeability have been examined experimentally [1,2]. The results indicate that water content in the hydrophilic polymer matrix decreases the T_g of the polymer, resulting in an extensive increase in gas permeation. Specifically, the oxygen permeability in EVOH increases nearly by two orders of magnitude as the relative humidity increases from 0 to 94% [1].

Molecular dynamics (MD) simulations have been used to study the effect of water on the permeation of oxygen and nitrogen through the poly(vinyl alcohol) (PVA) hydrogels that contain 27.5–80 wt% of water [3]. The diffusion of water in swollen PVA membranes has also been studied by MD simulations [4]. Our study will present the first MD simulation results on EVOH matrix, at least to our knowledge. We will focus on the oxygen permeability of EVOH-32 copolymer (32 mol% ethylene) with respect to the structural changes that take place in the amorphous matrix due to sorbed water molecules. Even though the crystalline domains act as barriers to penetrant movement in semi-crystalline polymers like EVOH, we will adopt the common procedure of modeling primarily the amorphous regions through which diffusion takes place and then introducing crystallinity effect based on crystallinity content. In contrast to previous simulations on PVA, the sorbed water content of EVOH is relatively lower, the maximum

* Corresponding author. Tel.: +90-212-358-1540 ext. 2365; fax: +90-212-257-5032.
E-mail address: doruker@boun.edu.tr (P. Doruker).

0032-3861/$ - see front matter © 2004 Published by Elsevier Ltd.
doi:10.1016/j.polymer.2004.03.024

value being 13 wt% that corresponds to 100% relative humidity condition.

2. Simulation details

Bulk structures of poly(ethylene-*co*-vinyl alcohol) (EVOH) were generated and simulated by using the commercial software of Accelrys (Insight II-Discover) [5] using the PCFF force field [6]. The calculations were performed on SGI Origin300 workstation.

2.1. Construction and equilibration of dry EVOH amorphous cell

Single chains of EVOH-32 (32 mol% ethylene), each containing 420 monomers and 2816 atoms in total, were formed by the POLYMERIZER module [5]. Random copolymer single chains were formed by using reactivity ratios of 1.0 for both vinyl alcohol and ethylene. The single chains were subsequently subjected to energy minimization.

The AMORPHOUS_CELL module of InsightII [5] was used to form amorphous (periodic) cells from the single chains by the method of Theodorou and Suter [7]. In order to avoid the generation of high-energy conformations due to long-range interactions, five bonds at a time were added to the growing chain end considering both bonded and non-bonded interactions. In order to minimize chain end effects, each cell contains only one polymer chain rather than several chains confined to the same volume, which would lead to an increased density of chain ends.

Amorphous cells were initially constructed at reduced densities of 0.88 g/cm^3. The increased free volume at the lower density was sufficient for the packing algorithm. Following the cell construction at the initial density, NPT dynamics was performed at 0.5 GPa and 300 K to bring the cells to the experimental density (ρ_{exp}) of EVOH. For this purpose, we needed an estimate of the amorphous density of semi-crystalline EVOH, since gas permeation occurs mainly through the amorphous regions.

The crystal structure of PVA is similar to that of polyethylene (PE) because the small CHOH group can fit into the PE crystal structure in place of a CH_2 group [8]. Therefore, we first calculated a crystalline density ($\rho_c = 1.45$ g/cm^3) for EVOH-32 using the orthorhombic unit cell structure of PE crystals. Then, an amorphous density ($\rho_a = 1.10$ g/cm^3) was estimated based on experimentally reported values [9] of overall sample density ($\rho = 1.174$ g/cm^3) and degree of crystallinity ($x_c = 0.27$) using the following relationship.

$$\frac{1}{\rho} = \frac{x_c}{\rho_c} + \frac{(1 - x_c)}{\rho_a} \quad (1)$$

The cohesive energy densities (CED) were evaluated for ten different amorphous cells formed by the above procedure, each containing a single chain with a different random sequence and conformation. The CED is computed as the difference between the energies of the single chain and the bulk system per volume. Then, the cell with the CED closest to the experimental value was chosen for further simulations. The evaluation of the chosen cell based on CED will be discussed in Section 3.1. This specific cell was refined by the Basic_Refine Protocol of Insight II [5], which employs an initial energy minimization, a brief NVT run at 300 K and a final energy minimization. Later annealing was performed by NPT dynamics procedure at 1 bar using the Temperature Cycle Protocol of Insight II [10]. During annealing, the cell was first heated by 50 °C increments from 300 to 750 K, which is well above the glass transition temperature of EVOH. Then the cell was cooled back to 300 K using 50 °C increments. The duration of the NPT dynamics simulations at each temperature was 5 ps.

The annealed cell was later put through a stage-wise equilibration procedure. First, the cell was pressurized at 300 K to increase its density well above the experimental one, and then the pressure was decreased in several stages to 1 bar. The aim was to obtain a refined system that would relax at the experimental density of the amorphous polymer at 1 bar and 300 K. Each stage consisted of three consecutive runs in the following order: (i) an NPT run at 300 K and a specific pressure, (ii) an NVT run at a high temperature well above T_g (750 K), and (iii) an NVT run at 300 K. The pressures of the NPT run (step (i)) at different stages were sequentially set at $P = 0.5$, 3.0, 1.0 and 0.5 GPa. Each of the three consecutive runs in all stages was applied for 50 ps.

Finally, the system was relaxed by NPT dynamics at 1 bar and 300 K for 100 ps to ensure that a constant density has been reached. The average cell density based on the final 30 ps of equilibration was 1.094 g/cm^3 with a corresponding cubic cell length of 29.3 Å on each side.

In all runs, Andersen method was used for temperature control [11]. In NPT runs, the pressure was controlled by Berendsen's method, where 0.1 ps and 0.5 GPa^{-1} were used as the pressure scaling constant (τ) and system compressibility value (β), respectively [12]. During these simulations, the cutoff distance for the non-bonded interactions was taken as 14 Å with respective spline and buffer widths of 2 and 1.5 Å. The time step was 1 fs in all stages. The relatively large cutoff distance might lead to some degree of contraction for the single chain at room temperature, not representing the unperturbed dimensions in the melt. However, the high density with periodic boundary conditions must screen out most of the long-range interactions, and possibly reduce the importance of the chain contraction effect. Moreover, the CED value for the amorphous cell is very close to the predicted values by group contribution methods (see Section 3.1).

2.2. Insertion of water and oxygen molecules. Further equilibration

The water sorbed by EVOH-32 copolymer (21% ethylene by weight) at 100% relative humidity condition is reported as 13.0 ± 1.1 wt% as a result of thermogravimetry experiments [13]. And at 28.3% relative humidity, the water content is given as 4.3 ± 1.2 wt% [13]. In our study, two relatively different weight percentages of water sorption, namely 3 and 13%, are chosen (3 g water/100 g EVOH and 13 g water/100 g EVOH). In order to obtain these specific water contents, 27 and 119 water molecules have to be inserted in the equilibrated dry EVOH cell, respectively.

The equilibrated EVOH cell was used for the construction of hydrated cells with two different concentrations. The water molecules were inserted at the free volume sites of the cell. The hydrated systems were subjected to energy minimization first by fixing the polymer atoms and afterwards by setting them free again. Even though the dry EVOH structure was built and equilibrated at 300 K, we later increased the simulation temperature to 323 K, in order to speed up the dynamics and see more jumps during the long NVT dynamics. That is why the temperature of the minimized EVOH cells with inserted water molecules was set to 323 K during the equilibration procedure and the NVT dynamics.

After insertion of water molecules to obtain the 3% water–EVOH system, an NVT dynamics of 1 ns is performed (at 323 K), then the system was relaxed by NPT dynamics at 1 bar for 1 ns, until the density of the system reached a constant value of 1.080 g/cm^3. Then the free volume sites of the system were detected and 10 oxygen molecules were placed at these sites in such a way that the distance between any pair of O_2 was at least 9 Å. The energy of the system with the O_2 molecules was then minimized followed by an NVT dynamics of 100 ps. The system was then relaxed by NPT dynamics at 1 bar until a constant density was obtained (about 300 ps). The resulting density of the 3% water–EVOH system with 10 O_2 molecules was 1.090 g/cm^3 at a temperature of 323 K.

In the case of 13% water–EVOH system, the insertion of water molecules was performed in two different stages. First 73 water molecules were inserted into the system by following the same procedure described above (8% water content). The system was equilibrated using the same procedure of the 3% water–EVOH system. Once the cell density reached a constant value, 46 more water molecules were added into the system and this increased the water weight percentage to 13%. After the application of the same equilibration procedure, the system relaxed at a constant density of 1.076 g/cm^3. Then 10 O_2 molecules were inserted into the system. After energy minimization and NPT relaxation (at 1 bar for 500 ps) stages, the system density again stabilized at a constant value of 1.080 g/cm^3 at a temperature of 323 K.

For the investigation of the diffusivity of oxygen molecules in the dry EVOH, 10 oxygen molecules were inserted at the free volume sites of the equilibrated EVOH cell structure such that the distance between any pair of oxygen was at least 9 Å. After insertion of oxygen molecules, the system was subjected to energy minimization. The resulting density of EVOH cell including the oxygen molecules was 1.100 g/cm^3. In order to be able to speed up the dynamics, the temperature of the system was similarly increased to 323 K.

2.3. MD simulations

All the three equilibrated EVOH cells containing oxygen molecules (EVOH-dry, EVOH–3% water, EVOH–13% water) were later subjected to NVT dynamics for 7 ns. In these simulations, the RATTLE method [14] was used to constrain the bond lengths allowing an integration time step of 2 fs. The temperature was controlled at 323 K by velocity scaling. The cutoff distance for non-bonded interactions was set to 12 Å, using respective spline and buffer widths of 2 and 1.5 Å. The trajectories were recorded at 1 ps intervals for further analysis.

3. Results and discussion

3.1. Evaluation of generated cells

As mentioned before, the density of the equilibrated dry EVOH cell is 1.094 g/cm^3 at 300 K, which is very close to the predicted density of amorphous EVOH (ρ_{exp} = 1.10 g/cm^3).

The solubility parameter is defined as $\delta = (\Delta E/V)^{1/2}$, where ΔE is the cohesive energy and V is the molar volume. The solubility parameter of 24.1 (MPa)$^{1/2}$ computed for the dry cell is slightly lower than the range of values: δ = 25.8–27.5 (MPa)$^{1/2}$, estimated by group contribution methods [15].

Based on these data, we can say that the dry equilibrated cell reasonably represents the amorphous structure of EVOH. Moreover, in the last section of this paper, we will also show that the glass transition temperatures of EVOH cells (dry and containing 13% water) predicted by MD simulations are consistent with experimental data. Therefore, we will proceed with the analysis of oxygen diffusion in these dry and hydrated EVOH cells, and then show the differences in the local equilibrium and dynamic properties of these cells.

3.2. Oxygen and water diffusion

Fig. 1 shows the displacements of three representative oxygen molecules (out of 10 penetrants) chosen from each structure as a function of time. Fig. 1(a)–(c) are for EVOH cells with 13, 3 and 0% water, respectively. For better

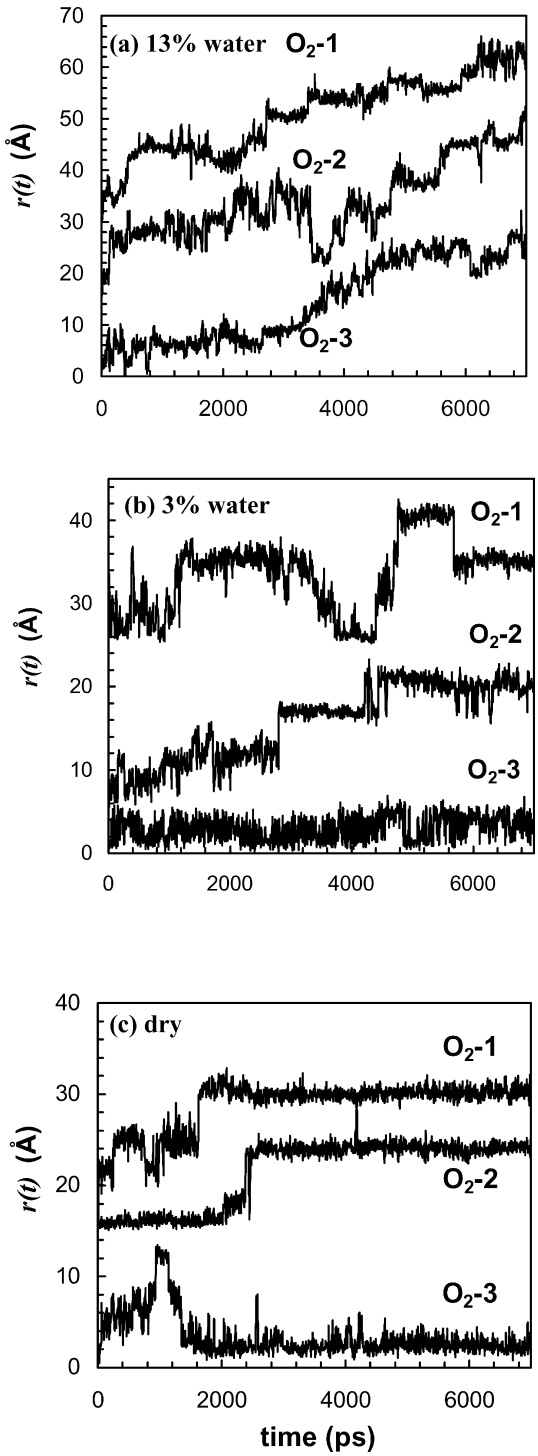

Fig. 1. Displacement of oxygen molecules in EVOH systems at 323 K with (a) 13% water (b) 3% water (c) dry.

visualization, the curves for O_2-1 and O_2-2 molecules have been shifted vertically by 25 and 5 Å in Fig. 1 (a), by 30 and 15 Å both in Fig. 1(b) and (c), respectively. In all cases, the hopping mechanism is the underlying process of the diffusion.

In the 13% hydrated system, the displacements of oxygen molecules are like in rubbery matrices and all the 10 oxygen molecules in the system make jumps leading to total displacements of within 10–35 Å within 7 ns. In the case of 3% water, three out of 10 oxygen molecules make no jumps at all during the 7 ns, e.g. O_2-3 of Fig. 1(b). While some oxygen molecules of the 3%-system, e.g. O_2-1 of Fig. 1(b), are showing back-and-forth hopping between the neighboring free volume sites as in the case of glassy polymers; some of them behave like in the rubbery matrices (e.g. O_2-2) [16,17]. This might result from the non-uniform distribution of the relatively few number of water molecules in the matrix. When there is no water in the system, the oxygen molecules either make no jumps or not more than two jumps. In summary, the oxygen molecules in the glassy EVOH matrix start to move like in the rubbery polymer matrices as the water content in the system increases.

The mean square displacement (MSD) of penetrants in the matrix over time t is given by $\langle r(t)^2\rangle = \langle(\boldsymbol{r}(t) - \boldsymbol{r}(0))^2\rangle$. Here, the brackets indicate an average taken for all penetrants over all time origins. The MSD of oxygen molecules in the three EVOH cell structures is shown in Fig. 2 on a logarithmic scale. The MSD of the oxygen molecules increases as the water content in the system increases. As observed in Fig. 1(c), all the jumps in dry EVOH take place in the initial 2.5 ns of the 7 ns trajectory, which indicates that there is further equilibration taking place in the matrix after the insertion of oxygen molecules. Therefore, in Fig. 2 the MSDs are plotted by discarding the first 2 ns of the trajectories.

The diffusion coefficient, D, of oxygen can be calculated by means of the Einstein relation

$$D = \frac{\langle r(t)^2\rangle}{6t},\ t \to \infty \tag{2}$$

In Fig. 2, the slope of log(MSD) vs. log(t) curve increases approximately to unity after 1 ns for the EVOH 13% water (the thin line with the slope 1.0 is shown) and the estimated diffusion coefficient of O_2 is found to be 1.0×10^{-6} cm^2/s at 323 K. The experimental oxygen diffusion coefficients of

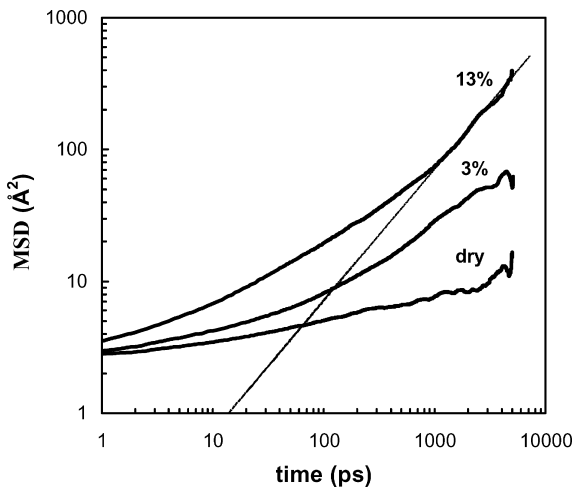

Fig. 2. Logarithmic plot of MSD vs. time for the diffusion of O_2 molecules in EVOH (13, 3 and 0% of water) at 323 K.

EVOH have not been reported. However, the diffusion coefficients of oxygen in PVA hydrogels have been computed for various water concentrations (27.5–79.7%) at 300 K [18]. A value of 8.0×10^{-8} cm^2/s at 300 K can be extrapolated for 13% water concentration in PVA, which is nearly 12 times lower than the computed value in this study. For dry EVOH and EVOH–3% water, the Einstein diffusion regime is not reached. We should also state that the diffusion of oxygen molecules in EVOH–13% water, is either one or two-dimensional rather than three, so the reported value is tentative. Longer trajectories would be necessary to achieve three-dimensional diffusion and to convincingly show diffusive behavior for this case and for what follows next on water diffusion.

The MSD of water molecules in the EVOH matrices with 3 and 13% water content is shown as a function of time during the 7 ns trajectories in Fig. 3. As the water content in the matrix increases, the MSD of water also increases. The slope of log(MSD) vs. log(t) curve is represented by the thin lines in Fig. 3. The slope increases approximately to unity after 2.5 ns and to 0.91 after 1.8 ns for EVOH with 3 and 13% water, respectively. The estimated diffusion coefficient of H_2O in EVOH with 3% water is 2.1×10^{-7} cm^2/s (only tentative, since total MSD is not comparable to box length), and it is 2.5×10^{-6} cm^2/s in EVOH with 13% water. These diffusion coefficients are consistent with the following values estimated for water in PVA [4]. At 300 K, the diffusion coefficient of H_2O in PVA was found in the range of $3–6 \times 10^{-7}$ cm^2/s for a water content of 11.6 wt%. At 375 K, it was found to be 3×10^{-7} cm^2/s in PVA containing 3.2 wt% water.

3.3. Solubility and permeability

The solubility coefficients of oxygen in PVA hydrogels are reported to increase about four times as the water weight

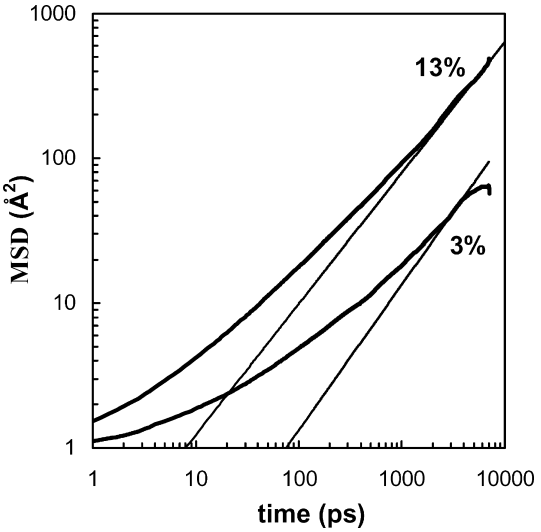

Fig. 3. Logarithmic plot of MSD vs. time for the diffusion of water molecules in EVOH with 3 and 13% water by weight at 323 K.

percentage decreases from 79.7 to 27.5 [18]. In our case, the solubility coefficient, S, of oxygen in the EVOH matrix is computed by the transition state approach (TSA) [19–21]. The details about the procedure and parameters of TSA can be found in our previous study [17]. The solubility coefficient of oxygen in dry EVOH is found to be about twice that in hydrated EVOH with 13% water.

The dry EVOH has very low oxygen permeability; therefore the experimental permeability measurements take a long time and exhibit variations larger than one order of magnitude [1,22]. In general, it has been found experimentally that 100% relative humidity increases the oxygen permeability of EVOH within one to two orders of magnitude, which is mainly due to the increase in the oxygen diffusion coefficients. This is in conformity with our simulation results, which indicate that the influence of relative humidity on the oxygen solubility value is much smaller compared to its effect on the diffusion coefficients.

In this study, the permeability coefficient of oxygen ($P = DS$) is found as 9.5×10^{-13} cm^3(STP) cm/cm^2 Pa s at 323 K and at 100% relative humidity by considering only the amorphous regions of EVOH-32. However, the effects of tortuosity and chain restriction due to crystalline regions should also be taken into account in the calculation of permeability. Here, we will use the following correlation developed for the permeability coefficient of semi-crystalline polymers [23]:

$$P = D_a S_a (1 - x_c)^2 \tag{3}$$

In this relationship, D_a and S_a are the respective diffusion coefficient and solubility of the amorphous region, and x_c is the sample's degree of crystallinity. To compare our computed permeability with the experimental value reported [1], we need to know x_c for the specific sample with 13% water (not reported in Ref. [1]). Comparison of the permeability value in Ref. [1] and the empirical relationship developed in Ref. [9] for permeability of similar EVOH samples as a function of crystallinity (both at 20 °C), a tentative crystallinity of 27% is estimated. Based on this x_c, our P_{sim}/P_{exp} factor becomes 79 (based on the maximum crystallinity value of 70% reported for EVOH samples [9], P_{sim}/P_{exp} ratio is 13). Of course, this comparison is only tentative due to several reasons. First of all our computed diffusion coefficient would be more reliable if extracted from a longer simulation. Second, the effect of crystallinity on permeability is based on an indirectly estimated crystallinity content and Eq. (3). Lastly, the swelling of the amorphous regions due to water content could be restrained by the presence of crystalline regions, which is not accounted for in our model. On the other hand, the fact that the glass transition temperatures computed for dry EVOH and EVOH with 13% water are in close conformity with experimental values (see Section 3.7) indicate that the generated cells reliably represent the amorphous structure.

3.4. Pair correlation functions

In order to understand the effect of relative humidity on the structure of EVOH matrix, the pair correlation (radial distribution) functions, $g(r)$, between the oxygen atoms of water molecules and the oxygen atoms in EVOH chain are shown in Fig. 4(a). The $g(r)$ shows a sharp peak for both water concentrations at a distance of $\approx$2.85 Å, indicating hydrogen bonding. The height of this peak for 3% water concentration is higher than that for 13%. Fig. 4(b) shows the pair correlation functions among different water molecules (oxygen atoms) residing in the same cell for EVOH with 3 and 13% water. The high peaks located at about 2.85 Å indicate that there is self-aggregation among water molecules. The height of the peak for EVOH–3% water is higher than that for EVOH–13% water. However, it should be stressed that these peaks indicate the normalized probability of water molecules making hydrogen bonds. If the total number of hydrogen bonds in both systems were counted, it would be higher in 13%-EVOH.

The distribution of water molecules at the end of 7 ns in both of the cell structures is compared in Fig. 5, where the polymer chain is not shown. The oxygen molecules are represented in blue color and the oxygen atom and the hydrogens of the water molecules are shown in red and white colors, respectively. In Fig. 5(a) the water molecules form clusters in different regions (3% water content) and

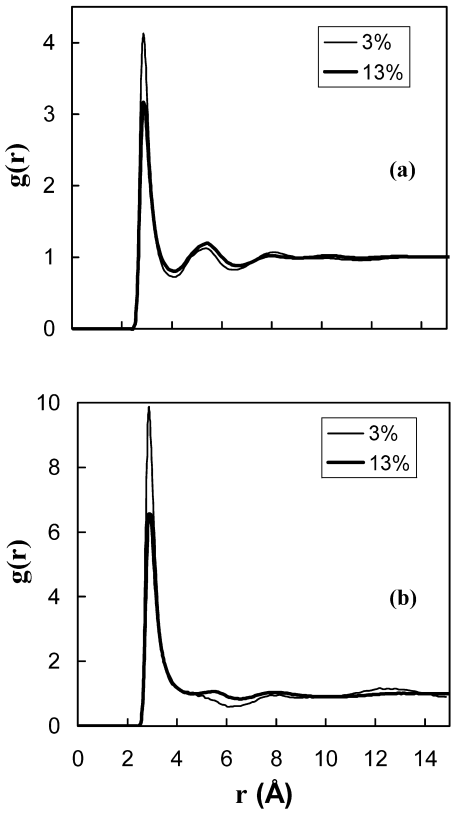

Fig. 4. The intermolecular $g(r)$ of the oxygen atoms of water (a) with oxygen atoms of EVOH (b) among themselves in EVOH cells.

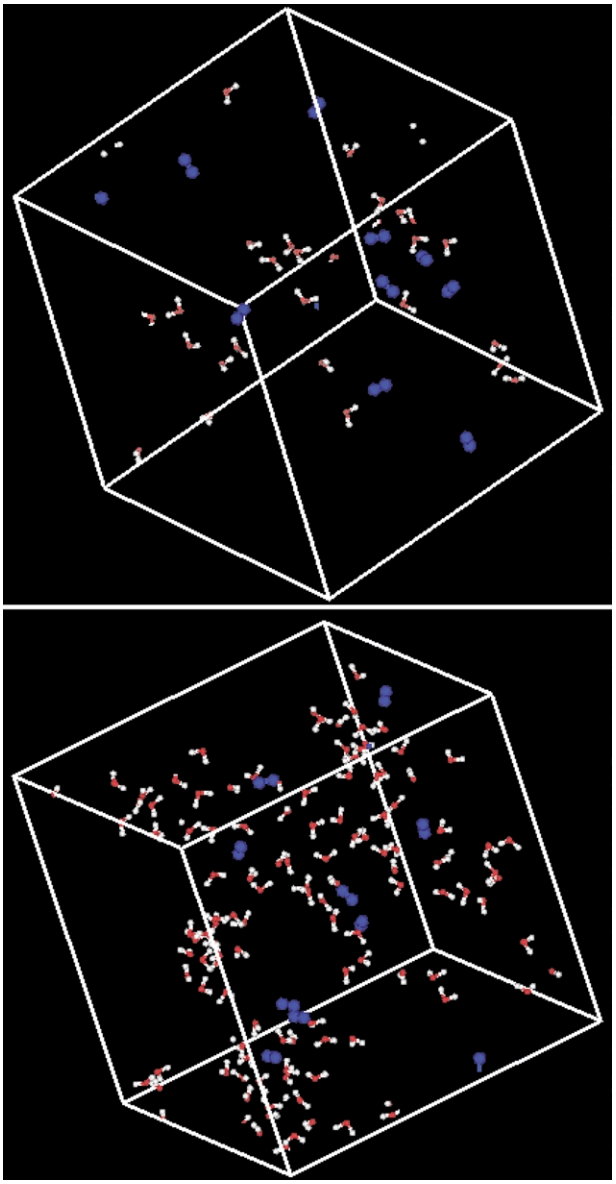

Fig. 5. The distribution of water and oxygen molecules in EVOH cells containing 3% water (top panel), and 13% water (bottom panel), excluding the polymer chain.

there are very few water molecules that do not belong to a cluster. In contrast in Fig. 5(b), where the water content is 13%, relatively more water molecules seem to lie in the pathways between the water clusters. Similar behavior has been observed by Tamai et al. for hydrogel models of PVA [24].

To see the effect of water molecules on the intermolecular interactions of the polymer chain, the intermolecular $g(r)$ between the oxygen atoms of the main chain is shown in Fig. 6. The intermolecular $g(r)$ shows a maximum around 2.85 Å indicating hydrogen bonding between OH groups of the EVOH polymer chain. In the case of a single polymer chain packed into the amorphous cell, the intermolecular $g(r)$ is based on the interactions of the chosen atoms (i.e. oxygen atoms) on the polymer chain with similar atoms on

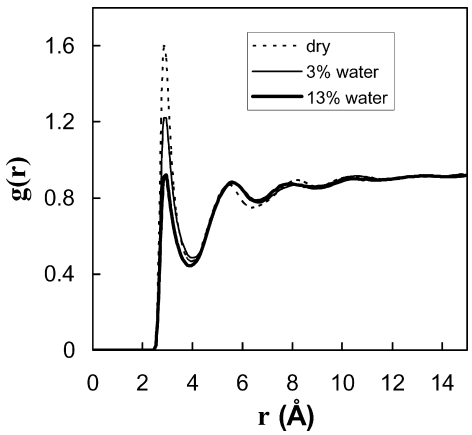

Fig. 6. The intermolecular $g(r)$ of OH groups of the main chain for EVOH-dry, EVOH–3% water and EVOH–13% water.

its periodic images [25]. The probability of the intermolecular interactions, given by the height of the peaks, compare in the three different systems as EVOH-dry > EVOH–3% water > EVOH–13% water. As the water content increases, the intermolecular hydrogen bonding decreases which may in turn lead to affect polymer chain mobility and cavity sizes.

Moreover, fictitious solubility parameters, δ_{sim}, are calculated for the hydrated systems after removing the water and oxygen molecules in order to make a comparison with the dry system. So this would give an idea about how much the cohesive energy of the matrix decreases as a result of structural changes. Table 1 lists solubility parameters at the end of 7 ns for each system without water and oxygen molecules, indicating a decrease in the cohesion of the matrix with increasing water content.

As a final remark, it might be expected that clustering of water molecules (Fig. 4(b)) should lead to the reduction of diffusion coefficients, due to an increase in the activation energy for making a diffusion step. However, the opposite situation prevails. The disruption of the hydrogen bonds among OH groups of EVOH by the presence of water molecules (Fig. 6), which also decreases the cohesion of the matrix, seems to be more effective on penetrant diffusion than the clustering of water molecules within free volumes. This seems consistent with the events occurring at the molecular scale, i.e. the hopping of the penetrants between different free volume sites or voids. Since the ease of passage from one void to a neighboring one would govern the displacement (or diffusion) of penetrants, factors that affect the opening/closing of pathways between voids, such as cohesion of the matrix and chain mobility, should be more effective on diffusion rather than the free volume content and sizes [17].

Table 1
Cavity volume percentage in the cells excluding the penetrants and $\delta_{(sim)}$ of the cells at the end of MD run

	Cavity volume %		
Time	Dry	3%	13%
2 ns	5.6	11	25.7
5 ns	6.3	10	26.3
7 ns	5.6	10	26.3
	$\delta_{(sim)}$ [a] $(MPa)^{1/2}$		
7 ns	23.9	22.2	19.1

[a] $\delta_{(sim)}$ is the simulated solubility parameter at the end of MD run. In the case of hydrated cells, the cohesive energy density is calculated after removing the water and oxygen molecules.

3.5. Cavity sizes

The free volume distributions in the cell structures of EVOH-dry, EVOH-3% and EVOH–13% water have been calculated at the end of 2, 5 and 7 ns using TSA with He gas as the probe molecule [19–21]. The same procedure used in our previous study was followed for the estimation of total cavity volume and the cavity volume fraction [17]. However, in this study water and oxygen molecules inside the cells have been removed first, and then the total free volume and the free volume distribution of the remaining cell structures, which consist of only the EVOH polymer chain, are calculated. This actually reveals the sizes of cavities that the penetrants reside in. Table 1 lists the ratio of total cavity volume to the total amorphous cell volume for each snapshot. The total volume percentage of the cavities increases drastically from 5–6% to 26% in the comparison of dry and 13% water containing EVOH.

Fig. 7 shows the volume fractions (f_a) of cavities that have sizes equal or greater than a threshold cavity volume. The fractions are based on the total cavity volume of each cell. Fig. 7 plots f_a as a function of threshold cavity size, and the following trend is observed: f_a (EVOH-dry) $\leq f_a \times$ (EVOH–3% water) $< f_a$ (EVOH–13% water). Three different snaphots at the end of 2, 5 and 7 ns (same as in Table 1) are plotted for each system, indicating that the free

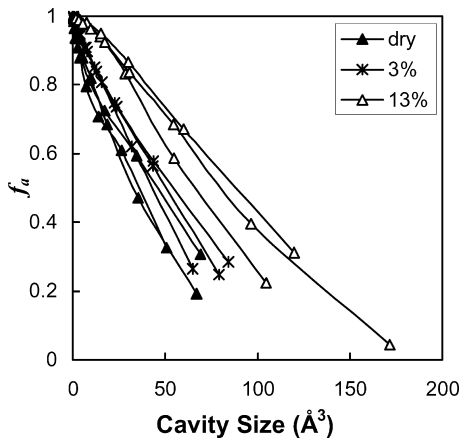

Fig. 7. Cavity volume fraction, f_a, as a function of threshold cavity size for EVOH-dry, EVOH–3% water, EVOH–13% water. For each system three different distributions are provided for snapshots at the end of 2, 5, and 7 ns.

volume distributions are not static during the trajectories. There is a significant increase in f_a of the EVOH cell with 13% water compared to the structures of the other two systems. This significant increase occurs due to the hydrogen bond weakening and gradual swelling of the polymer ending up in enlarging the volume of the cavities. The difference between the cavity volume distributions of EVOH with 13% water and the other two systems (EVOH–3% water and EVOH-dry) would indicate a decrease in glass transition temperature. It has been observed by Hodge et al. that poly(vinyl alcohol) samples with water content greater than 8% by weight show larger free volume cavities due to the swelling of the polymer [26]. The swelling causes plasticization of the polymer and decreases the T_g.

In general, the solubility of small gas molecules in the amorphous polymer systems decreases, as the free volume percentage of the system reduces. In our case, the computed solubility value of the oxygen in the matrix of EVOH–13% water content is lower by a factor of 2 compared to the dry matrix, which seems to conflict with the increased size of the cavities at first site. However, the cavities are filled with water molecules. When the water molecules are not removed from the matrix, the total free volume of the EVOH–13% water is found to be 5.3%, similar to the total free volume content of the dry system.

3.6. Local chain mobility

The water molecules interacting with the polymer OH groups reduce the inter-chain hydrogen bonds of EVOH (Fig. 6), resulting in increased volume of the cavities in the matrix. The weakening of inter-chain hydrogen bonding should also affect the local chain mobility. To observe this effect, the rotational (orientational) time correlation function is calculated [27,28].

$$m(t) = \langle \boldsymbol{u}(t_0)\cdot\boldsymbol{u}(t_0 + t)\rangle \tag{4}$$

Here $\boldsymbol{u}(t)$ denotes a unit vector that characterizes the orientation of the main or side chain of the polymer at a given time, t. The ensemble average is evaluated on the basis of an ensemble of snapshots at various starting times, t_0.

The local relaxation of the EVOH chains is monitored by looking at the bond vectors connecting C(i) and C($i+1$) atoms on its backbone. Fig. 8 compares the relaxation behavior of the three systems. Interestingly, there is no considerable difference between the dry EVOH and EVOH with 3% water. In contrast, the local relaxation of EVOH with 13% water is much faster compared to the other matrices. This indicates that at 13% water concentration the reduction in the number of interchain hydrogen bonds and the increase in cavity sizes enhance local mobility. The experimental results of Hodge et al. have indicated that maximum main chain mobility is reached only after a certain level of plasticization [26]. In our case, the higher free volume content and faster chain mobility of EVOH

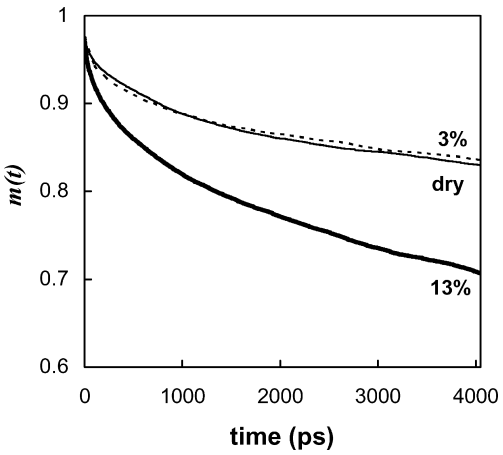

Fig. 8. The rotational time correlation function for the main chain bond vectors of EVOH-dry, EVOH–3% water, EVOH–13% water.

with 13% water are the two indications that the polymer is in its rubbery state.

The relaxation times, τ, are also obtained by fitting $m(t)$ to the empirical Williams–Watts expression, where $\beta = 1$ [18].

$$m(t) = A\exp[-(t/\tau)^{\beta}] \tag{5}$$

The fitting is performed for the time range of 0–1 ns. τ values for EVOH-dry, EVOH-3% and EVOH–13% water are found to be 11.3, 11.2 and 6.0 ns, respectively.

3.7. Glass transition temperature

The glass transition temperature of EVOH with 13% water is determined from MD simulations (NPT ensemble) and compared with that of the dry EVOH. To find the T_g from simulation, the temperature of the equilibrated cell is lowered stepwise from 300 K to a temperature of 238 K for the dry EVOH (160 K for EVOH with 13% water) using the final equilibrium cell obtained at higher temperature as the starting structure for dynamics at the next lower temperature. Similarly, the temperature is raised stepwise from 300 K to a temperature of 420 K for the dry EVOH (360 K for EVOH with 13% water). At each temperature, the polymer cell is subjected to 200 ps NPT dynamics, while the last 150 ps of dynamics is used to determine the specific volume.

The glass transition temperatures for the two matrices are determined from plots of specific volume vs. temperature, as shown in Fig. 9. In each case, a line is drawn through the data points falling above and below a temperature of 330 K for EVOH-dry and 240 K for EVOH–13% water. And the glass transition temperature is located at the intersection of the two lines.

In general, the simulation results are consistent with experimental values of T_g. For dry EVOH, our simulations indicate a value of 324 K, which falls between the two experimentally reported T_g values of 318 K [13] and 334 K

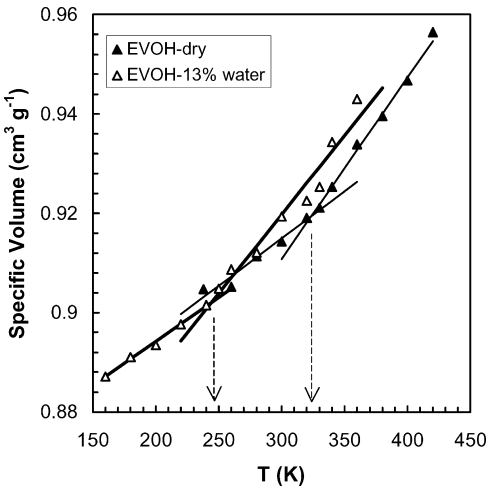

Fig. 9. Plots of specific volume of EVOH-dry and EVOH–13% water vs. temperature obtained by NPT dynamics.

[29]. Similarly our computed T_g value of 243 K for EVOH with 13% of water is between reported values of 213 K [13], and 255 K [29].

The computations and experiments both indicate a marked drop of about 80–100 °C in the glass transition for EVOH with 13% of water. This drop in T_g is indicative of plasticization of the EVOH matrix, which results from the weakening of intermolecular hydrogen bonds of the EVOH chain, leading to larger cavities and increased chain mobility on a molecular scale.

4. Concluding remarks

MD simulations indicate that high water content results in a noticeable increase in the oxygen and water vapor permeability of the EVOH copolymer as the water content increases up to 13% by weight. It is found out that the water molecules form hydrogen bonds with the side groups of EVOH and disrupt the intermolecular hydrogen bonds among the EVOH chains. As a result, local chain mobility increases and the glass transition temperature is reduced by about 80 K. The oxygen molecules start to jump like in rubbery polymers and the diffusion coefficients of oxygen and water increase appreciably.

Moreover, with increasing water content, the cavity sizes in the EVOH enlarge. However, since these cavities are filled with water molecules, the solubility values of oxygen molecules in the EVOH in fact decrease as a result. Therefore the increase in permeability seems to mainly result from the increase in the diffusion.

One unexpected finding is that the local chain relaxation of the dry EVOH and EVOH–3% water are almost identical. And the local relaxation shows a marked increase at 13% water content. However, a continuous increase in the diffusion of oxygen molecules is observed with increasing water content. This indicates that other parameters, such as disruption of intermolecular hydrogen bonding and the increase in cavity sizes, are dominant in determining the difference between the oxygen diffusion rates in the dry EVOH and EVOH–3% water.

Our simulations focus on the structural changes that take place in the amorphous regions of EVOH due to water sorption and its effects on permeability. The crystalline content is neglected in our simulations, which could have been included by mesoscale simulations [30]. However, the neglect of crystallinity has been commonly adopted in MD simulations on other semi-crystalline polymers such as polyethylene [31,32], since it is known that gas diffusion primarily occurs in amorphous regions and crystals act as barriers to gas diffusion. In general, the amorphous EVOH structures generated in this study seem reliable since the CED, and glass transition temperatures are correctly estimated. As a result, we can state that the structural changes in the amorphous matrix observed here at the atomistic scale should be pertinent in explaining the changes in permeability at least qualitatively.

Acknowledgements

This work has been supported by the Bogazici University B.A.P. (Projects 03A501-D and 03R104), DPT Project (01K120280), and the Turkish Academy of Sciences in the framework of the Young Scientist Award Program (PD-TUBA-GEBIP/2002-1-9).

References

[1] Zhang Z, Britt IJ, Tung MA. J Appl Polym Sci 2001;82:1866.
[2] Zhang Z, Britt IJ, Tung MA. J Polym Sci Part B: Polym Phys 1999;37:691.
[3] Tamai Y, Tanaka H. Fluid Phase Equilib 1998;144:441.
[4] Müller-Plathe F. J Membr Sci 1998;141:147.
[5] Accelrys Inc, San Diego, CA, USA (Insight II 4.0.0 P+, POLYMERIZER, DISCOVER, AMORPHOUS_CELL, BUILDER and RIS Modules version 2001.11).
[6] Sun H, Mumby SJ, Maple JR, Hagler AT. J Am Chem Soc 1994;116:2978.
[7] Theodorou DN, Suter UW. Macromolecules 1985;18:1467.
[8] Billmeyer FW. Textbook of polymer science, 3rd ed. USA: Wiley; 1984.
[9] Armstrong RB. TAPPI 2002, PLACE Conference; 2002.
[10] Sok RM, Berendsen HJC, van Gunsteren WF. J Chem Phys 1992;96:4699.
[11] Andersen HC. J Chem Phys 1980;72:2384.
[12] Berendsen HJC, Postma JPM, van Gunsteren WF, DiNola A, Haak JR. J Chem Phys 1984;81:3684.
[13] Aucejo S, Marco C, Gavara R. J Appl Polym Sci 1999;74:1201.
[14] Andersen HC. J Comput Phys 1983;54:24.
[15] Brandrup J, Immergut EH, Grulke EA. Polymer handbook, 4th ed. Canada: Wiley; 1999.
[16] Hofman D, Fritz L, Ulbrich J, Paul D. Comput Theor Polym Sci 2000;10:419.
[17] Kucukpinar E, Doruker P. Polymer 2003;44:3607–20.
[18] Tamai Y, Tanaka H. Fluid Phase Equilib 1998;144:441.

[19] Gusev AA, Arizzi S, Suter UW, Moll DJ. J Chem Phys 1993;99:2221.
[20] Gusev AA, Arizzi S, Suter UW. J Chem Phys 1993;99:2228.
[21] Gusev AA, Müller-Plathe F, van Gunsteren WF, Suter UW. Adv Polym Sci 1994;116:207.
[22] Plastics Design Library, Permeability and other film properties, 2nd ed. New York: William Andrew Inc; 1996.
[23] Van Krevelen DW. Properties of polymers. The Netherlands: Elsevier Science Publishers; 1990.
[24] Tamai Y, Tanaka H, Nakanishi K. Macromolecules 1996;29:6750.
[25] Krishna Pant PV, Han J, Smith GD, Boyd RH. J Chem Phys 1993;99: 597.
[26] Hodge RM, Bastow TJ, Edward GH, Simon GP, Hill AJ. Macromolecules 1996;29:8137.
[27] Allen MP, Tildesley DJ. Computer simulation of liquids. Oxford: Clarendon Press; 1991.
[28] Bahar I, Badur B, Doruker P. J Chem Phys 1993;99:2235.
[29] Lagaron JM, Powell AK, Bonner G. Polym Test 2001;20:569.
[30] Baschnagel J, Binder K, Doruker P, Gusev AA, Hahn O, Kremer K, Mattice WL, Müller-Plathe F, Murat M, Paul W, Santos S, Suter UW, Tries V. Adv Polym Sci 2000;152:41.
[31] Müller-Plathe F. J Chem Phys 1991;94:3192.
[32] Fukuda M, Kuwajima S. J Chem Phys 1997;107:2149.